Ionospheric Anomalies Associated with Mw7.3 Iran-Iraq Border Earthquake and a Moderate Magnetic Storm

Erman ŞENTÜRK[1], Samed INYURT[2], İbrahim SERTÇELİK[3]

[1]Department of Geomatics Engineering, Kocaeli University, Turkey
[2]Department of Geomatics Engineering, Gaziosmanpaşa University, Turkey
[3]Department of Geophysical Engineering, Kocaeli University, Turkey

Correspondence: Erman Şentürk (erman.senturk@kocaeli.edu.tr)

Abstract. The analysis of the unexpected ionospheric phases before large earthquakes is a popular approach in earthquake prediction studies. In this study, the Total Electron Content (TEC) data of ~~five~~ seven International GNSS Service (IGS) stations and the Global Ionosphere Maps (GIMs) were used. The Short-time Fourier Transform (STFT) and a running median process were applied on the TEC time series to detect abnormalities before the Mw7.3 Iran-Iraq border earthquake on November 12, 2017. The analyzes showed positive anomalies 8-9 days before the earthquake and some positive/negative anomalies 1-6 days before the earthquake. These anomalies were cross-checked by space weather indices Kp, Dst, F10.7, Bz component of the interplanetary magnetic field (IMF Bz), electric field (Ey), and plasma speed (V_{SW}). The results showed that the anomalies 1-6 days before the earthquake caused by a moderate magnetic storm. Also, the positive anomalies 8-9 days before the earthquake should be related to the Iran-Iraq border earthquake due to quiet space weather, local dispersion, and proximity to the epicenter.

1 Introduction

The ionosphere is a three-dimensional dispersive atmosphere layer. The layer locates above approximately 50-1000 km from the Earth's surface and includes molecules with potential for photoionization. When molecules are exposed to light energy emitted from the sun, their components are divided into atoms, which are electrons and a compact nucleus of protons and neutrons. Negatively charged electrons ~~The molecules are separated into protons and electrons when exposed to light energy emitted from the sun. Electrons separated from molecules~~ effect the propagation of electromagnetic signals traveling between space and earth. The degree of effect is a function of the number of free electrons. The sun is the primary determiner of the number of electrons and causes permanent and regular ionospheric trends such as daily, 27-day, seasonal, semi-annual, annual, and 11-year. The number of electrons also increase/decrease due to disturbed space-weather (Bagiya et al., 2009), earthquakes (Liu et al., 2004; Şentürk et al., 2018), tsunamis (Occhipinti et al., 2013), volcanic eruptions (Dautermann et al., 2009), hurricanes (Chou et al., 2017) and anthropogenic events (Lin et al., 2017). These events generally cause non-secular changes, which are commonly named as ionospheric disturbances/anomalies.

~~In recent decades, seismoionospheric studies have become quite popular. The first case was reported for Good Friday Alaska Earthquake of 1964 (Davies and Baker, 1965; Leonard and Barnes, 1965). In those years, data of ionosonde, radio waves, and topside sounding were used to analyze ionospheric anomalies before earthquakes (Gokhberg, 1983; Molchanov et al., 1992; Pulinets et al., 1998; Liu et al., 2000). Calais~~

~~and Minster (1995) firstly used GPS observations for seismoionospheric analysis of the Mw 6.7 Northridge earthquake.~~

Global Navigation Satellite System (GNSS) technology provides low-cost, high accuracy, near real-time, and continuous ionospheric data. GNSS based TEC data is preferred in many subsequent seismoionospheric studies related to large earthquakes (Liu et al., 2004, 2010; Fuying et al., 2011; Yildirim et al., 2016; Ulukavak and Yalcinkaya, 2017; Yan et al., 2017; Ke et al., 2018; Şentürk et al., 2018; Tariq et al., 2019). Liu et al. (2004) investigated 20 earthquakes with a magnitude greater than 6 in Taiwan between 1999 and 2002. They used the GPS based TEC data and applied the 15-days moving median and quartile range method to the TEC variation. The results showed that ionospheric abnormalities were detected before earthquakes, with an 80% success rate. Liu et al. (2010) reported seismoionospheric precursors of the 2004 M=9.1 Sumatra-Andaman Earthquake due to anomalous decreases in the TEC variation five days before the earthquake. Fuying et al. (2011) used the Kalman filter method to detect the abnormal changes of TEC variations before and after the Wenchuan Ms8.0 earthquake. The TEC data were calculated from the GPS observations observed by the Crustal Movement Observation Network of China (CMONOC). The result showed that the Kalman filter is reasonable and reliable in detecting TEC anomalies associated with large earthquakes. Yildirim et al. (2016) utilized 4 Continuously Operating Reference Stations in Turkey (CORS-TR) and 11 IGS and EUREF Permanent Network (EPN) stations to investigate the ionospheric disturbances related to Mw 6.5 offshore in the Aegean Sea earthquake on 24 May 2014. TEC data obtained from Precise Point Positioning (PPP) and Global Ionosphere Maps (GIMs)~~GIMs~~ showed that the TEC values anomalously increased 2-4 TECU 3 days before the earthquake and decreased 4-5 TECU on the day before the earthquake. Ulukavak and Yalcinkaya (2017) used GNSS based TEC data of 6 IGS stations to determine the pre-earthquake ionospheric anomalies before the Mw 7.2 Baja California earthquake on 4 April 2010. The results showed both positive and negative ionospheric anomalies occurred one to five days before the earthquake. Yan et al. (2017) utilized data of CMONOC and IGS to statistically investigate the TEC anomalies before 30 Mw6.0+ earthquakes from 2000 to 2010 in China. TEC anomalies were detected before 20 earthquakes, nearly 67%. Ke et al. (2018) used a ~~Linear~~ linear ~~Model~~ model between TEC and F10.7 ~~(LMTF)~~ to detect seismoionospheric TEC anomalies before and after the Nepal earthquake 2015. The method was compared with Sliding Quartile and Kalman filter methods. They found that the linear model ~~LMTF~~ is more effective in detecting the TEC anomalies caused by the Nepal earthquake in temporal and spatial. Şentürk et al. (2018) comprehensively analyzed the ionospheric anomalies before the Mw7.1 Van earthquake on 23 October 2011 with temporal, spatial, and spectral methods. The results showed a 2-8 TECU increase in the TEC time series of 28 GNSS stations and GIMs before the Van earthquake on 9 October, 15-16 October, and 21-23 October. Tariq et al. (2019) used GNSS based TEC data to detect seismoionospheric anomalies of three major earthquakes (M>7.0) in Nepal and the Iran-Iraq border during 2015-2017. The ionospheric precursors of three earthquakes generally occur within ten days, about 08:00-12:00 UT in the daytime. The temporal and spatial statistical tests showed that the abnormal positive TEC changes were detected nine days before the Mw7.3 Iran-Iraq earthquake.

There is still no consensus on the physical process of the changes in the ionosphere before earthquakes, but several assumptions have been made about the subject (Toutain and Baubron, 1998; Pulinets et al., 2006; Namgaladze et al., 2009; Freund et al., 2006, 2009; Freund, 2011). Toutain and Baubron (1998) reported that the radon and other gases from the earth's crust near the active fault progress toward the atmosphere and cause ionization. The increased radon release produces a non-pronounced heat release (increasing air temperature) in the atmosphere by connecting the water molecules to the ions. This increase in air

temperature leads to variability in air conductivity (Pulinets et al., 2006). The amount of electron density in the ionosphere increases/decreases by this chaining process. Freund et al. (2006) detected the ionization of the side surfaces of the block where the air was ionization by increasing the mechanical pressure applied to the upper surface of a granite block in the laboratory. With this assumption, strains occurring in the huge rocks in the lithosphere before the earthquakes can cause electron emission towards the atmosphere and may cause changes in the ionosphere (Freund et al., 2009).

In this study, the temporal, spatial, and spectral analysis was applied to the GNSS based TEC data to detect ionospheric anomalies before the Mw 7.3 Iran-Iraq border earthquake on November 12, 2017. The Short-time Fourier Transform (STFT) ~~STFT~~ and a running median process were applied to define abnormalities in the TEC time series. The indices Kp, Dst, F10.7, Bz component of the interplanetary magnetic field (IMF Bz), electric field (Ey), and plasma speed (V_{SW})~~IMF Bz, Ey, and V_{sw}~~ were also analyzed to show the effect of space weather ~~conditions~~ on TEC variation. The paper is organized as follows: In Section 2.1, information on the Iran-Iraq border earthquake is given. Section 2.2 includes data observations. In Section 2.3, GPS-TEC and GIM-TEC data calculations are described. In Section 2.4,~~ -~~the methods used in the study are explained capaciously. The results are given in Section 3, and Section 4 concludes the paper.

2 Data and Analysis

2.1 Iran–Iraq Border Earthquake

The deadliest earthquake of 2017, with at least 630 people killed and more than 8,100 injured occurred near the Iran–Iraq border (34.911°N, 45.959°E) with a moment magnitude of 7.3 at a depth of 19.0 km on November 12, 2017, at 18:18 UTC (U.S. Geological Survey, 2017). The earthquake was felt in Iraq, Iran, and as far away as Israel, the Arabian Peninsula and Turkey. The focal mechanism of the earthquake is pointed out as a thrust-faulting dipping at a shallow angle to the northeast. The earthquake occurred on the continental collision between Eurasian and Arabian Plates located within the Zagros fold and thrust belt.

2.2 The GNSS based TEC data

The GNSS TEC data of ~~five~~ seven IGS stations and GIMs produced by the Center for Orbit Determination in Europe (CODE) were used to investigate ionospheric anomalies before the Iran-Iraq border earthquake. The location of the IGS stations and the epicenter are shown in ~~Figure~~ Fig. 1. The five IGS stations are selected in the Earthquake Preparation Area (EPA) and the two IGS stations located far away from the epicenter to reveal earthquake-induced anomalies. EPA~~earthquake preparation area, which~~ is calculated by the Dobrovolsky equation, $r = 10^{0.43M}$ km, where M is the magnitude (Dobrovolsky et al., 1979) and it is found to be 1380 km for the Iran-Iraq border EQ. ~~. The earthquake preparation area of the Iran-Iraq border earthquake is found to be 1380 km.~~ The distance of IGS stations to the epicenter and other information are given in Table 1. The geomagnetic coordinates of the stations were obtained from the KYOTO website (http://wdc.kugi.kyoto-u.ac.jp/igrf/gggm/). Receiver Independent Exchange Format (RINEX) files of the IGS stations were downloaded from the IGS website (ftp://igs.ensg.ign.fr/pub/igs/data/), and Ionosphere Map Exchange Format (IONEX) files of CODE were downloaded from the National Aeronautics and Space Administration (NASA) website (ftp://cddis.gsfc.nasa.gov/gps/products/ionex/). The CODE GIMs covers $\pm 87.5^0$ latitude and $\pm 180^0$ longitude ranges with $2.5^0 x 5^0$ spatial resolution (5184 cells) and ~~2~~1-hour temporal resolution~~s~~ (Dach et al., 2020).

Table 1 Information on the stations

Site	Network	Country	Lat. (^{0}N)	Long. (^{0}E)	Geomag. Lat. (^{0}N)	Geomag. Long. (^{0}E)	Distance from the epicenter (km)
ankr	IGS	Turkey	39.8875	32.7583	36.54	112.72	1288.95
aruc	IGS	Armenia	40.2856	44.0856	35.27	123.34	619.95
bshm	IGS	Israel	32.7789	35.0200	29.23	113.25	1037.09
isba	IGS	Iraq	33.3414	44.4383	28.40	122.24	223.72
tehn	IGS	Iran	35.6972	51.3339	29.79	129.11	495.45
lroc	IGS	France	46.1589	-1.2193	48.23	81.47	4111.74
lhaz	IGS	China	29.6573	91.1040	20.27	164.94	4248.22

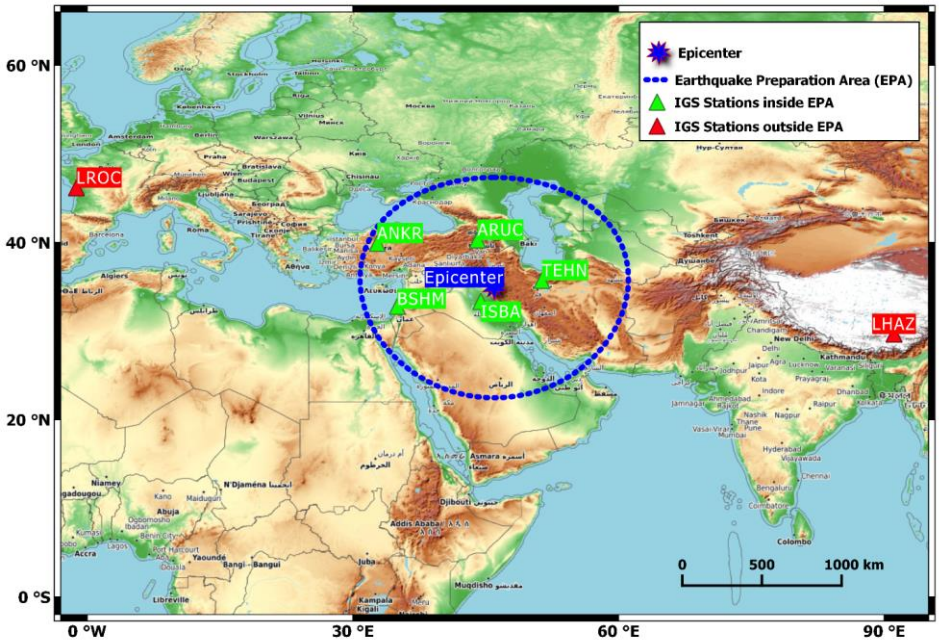

Figure 1. The epicenter of Iran-Iraq border earthquake and location of IGS stations (Map of the area is provided by https://opentopomap.org and it was composed in QGIS program).

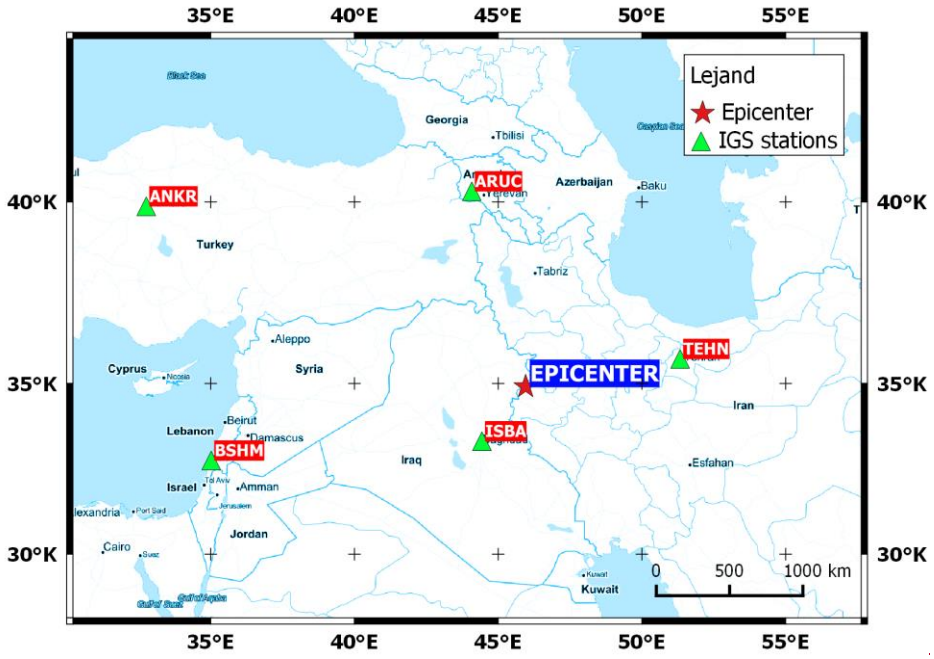

Figure 1. The epicenter of Mw 7.3 Iran-Iraq border earthquake and location of IGS stations (Map of the area is provided by http://maps.stamen.com and it was composed in QGIS program)

Biçimlendirilmiş: Ortadan

Table 1 Information on the stations

Site	Network	Country	Lat. (°N)	Long. (°E)	Geomag. Lat. (°N)	Geomag. Long. (°E)	Distance from the epicenter (km)
ANKR	IGS	Turkey	39.8875	32.7583	36.54	112.72	1288.95
ARUC	IGS	Armenia	40.2856	44.0856	35.27	123.34	619.95
BSHM	IGS	Israel	32.7789	35.0200	29.23	113.25	1037.09
ISBA	IGS	Iraq	33.3414	44.4383	28.40	122.24	223.72
TEHN	IGS	Iran	35.6972	51.3339	29.79	129.11	495.45

Biçimlendirilmiş: Aralık Önce: 0 nk

The TEC describes the number of free electrons in a cylinder with 1 m^2 base area throughout the line of sight (LOS). The unit of the TEC (TECU) is equal to 10^{16} electron/m^2. The linear integral of the electron density along the signal path ($\int_l Ne(\vec{r},t)ds$) corresponds to the Slant Total Electron Content (STEC). STEC depends on the signal path geometry from GNSS satellites (above 20.000 km height from the earth's surface) to a receiver. STEC is converted to the Vertical Total Electron Content (VTEC) with a mapping function.

This conversion provides the number of free electrons perpendicular to the earth. VTEC is used for the input data of the global and regional ionosphere models, and it is a more useful parameter to define all ionization in the ionosphere. Assuming all electrons are gathered in a thin layer, TEC values in the receiver's zenith azimuth is obtained by the weighted average of the VTECs of all visible satellites (Schaer, 1999).

The effect of the ionosphere to the GNSS signal is directly proportional to the number of free electrons throughout LOS and inversely proportional to the square of the frequency of the GNSS signals (Hofmann-Wellenhof et al., 1992). The TEC parameter can be calculated with at least two different frequencies of GNSS signals because the effect of the ionosphere during the signal transition depends on the signal frequency. In recent years, the TEC parameter is obtained from single-frequency receivers by Precise Point Positioning (PPP) technique in which some parameters in the TEC calculation model are derived from IGS (Hein et al., 2016; Li et al., 2019). In this study, the Geometry-Free Linear Combination (L_4=L_1-L_2) and "leveling carrier to code" algorithm is used to calculate TEC values of five seven IGS stations (Ciraolo et al., 2007). L_4 combination of carrier phase and code observations are as follows,

$$L_4 = L_1 - L_2 = -\alpha\left(\frac{1}{f_1^2}-\frac{1}{f_2^2}\right)STEC + \lambda_1 B_{1,i}^k - \lambda_2 B_{2,i}^k \quad (1)$$

$$P_4 = P_1 - P_2 = \alpha\left(\frac{1}{f_1^2}-\frac{1}{f_2^2}\right)STEC + c(\Delta b^k - \Delta b_i) \quad (2)$$

where α is a constant, f is the signal frequency, $\lambda B_i^k = \lambda\left(N_i^k + \delta N_i^k\right) + c(b^k + b_i)$ is the initial phase ambiguity (i and k indexes refer to receiver and satellite respectively), λ is the wavelength, N_i^k is an integer, δN_i^k is the effect of the phase wind-up, c is the speed of light, b^k is the satellite, and b_i is the receiver hardware delays (DCBs: Differential Code Biases). The DCBs of satellites and receivers are available in the daily IONEX files for IGS stations, but receiver DCBs of non-IGS stations must be calculated in the TEC calculation process. The phase leveling technique is based on differences carrier phase and code observations on a continuous arc to reduce ambiguities from the carrier phase (L_4).

$$\langle L_{4,arc} + P_4\rangle_{arc} \cong \lambda_1\delta N_1 - \lambda_2\delta N_2 = B_4 \quad (3)$$

$$L_4 = L_4 + \langle L_{4,arc} + P_4\rangle_{arc} = \alpha\left(\frac{1}{f_1^2}-\frac{1}{f_2^2}\right)STEC + b_4^k + b_{4,i} + B_4 \quad (4)$$

In Eq. 3, the carrier phase observations are leveled with a bias produced by phase ambiguity. Finally, the STEC is calculated using Eq. 5.

$$STEC = \alpha\left(\frac{1}{f_1^2}-\frac{1}{f_2^2}\right)^{-1}\left(L_4 - \left(B_4 + b_4^k + b_{4,i}\right)\right) \quad (5)$$

The STEC is converted to VTEC using the Single-Layer Model and a mapping function.

$$VTEC = STEC\sqrt{1-\left(\frac{R_E}{R_E+h_m}\right)^2 cos^2\,\varepsilon} \quad (6)$$

To define the number of free electrons in the receiver's azimuthzenith, TEC is generally calculated by the weighted average of the VTECs of all visible satellites (Çepni and Şentürk, 2016).

$$TEC = \frac{\sum_{i=1}^{N} W_i VTEC_i}{\sum_{i=1}^{N} W_i}\Bigg|_{T_1}^{T_2}$$; T_1-T_2 is time-lapse interval (7)

where Wi indicates the weight of a satellite, which is generally described as a component of the satellite elevation angle, i = 0,1,…,n and n is equal to the number of visible satellites at any epoch.

TEC values of the epicenter are interpolated from the nearest four grid points of GIMs using a simple 4-point bivariate interpolation (Schaer et al., 1998).

$$TEC(\lambda_e, \beta_e) = |1-m \quad m| \begin{vmatrix} VTEC_{00} & VTEC_{01} \\ VTEC_{10} & VTEC_{11} \end{vmatrix} \begin{vmatrix} 1-n \\ n \end{vmatrix} \quad (8)$$

$$m = |\lambda_e - \lambda_0| / \Delta\lambda_{GIM} \quad (9)$$

$$n = |\beta_e - \beta_0| / \Delta\beta_{GIM} \quad (10)$$

where m, n are latitudinal/longitudinal scale factor, β_e and λ_e is geocentric latitude/longitude of the epicenter, β_0 and λ_0 is geocentric latitude/longitude of the nearest grid point, $\Delta\beta_{GIM}$ and $\Delta\lambda_{GIM}$ are spatial resolutions of the latitude/longitude of the GIMs, $VTEC_{00}, VTEC_{01}, VTEC_{10}, VTEC_{11}$ are VTECs of the nearest grid points.

2.3 The Short-Time Fourier Transform and Running Median Methods

The STFT is a method of obtaining the signal frequency information in the time domain as a modified version of the classical Fourier (Gabor, 1946). The STFT provides the analysis of a small part of the signal at a particular time with the "windowing" technique (Burrus, 1995). The method divides the signal with a fixed time-frequency resolution (the size of the window is fixed in all frequencies) and presents the results in the time-frequency domain. It provides information about both when and at which frequencies a signal occurs. In this way, the method can provide statistical information about where and when the abnormality occurs in a TEC time series. The STFT of a signal is calculated by Eq.11.

$$STFT(\tau, f) = \int_{-\infty}^{+\infty} f(t) g(t-\tau) e^{-i\omega t}\, dt \quad (11)$$

where f(t) is a time series (e.g., TEC), g(t) is the window function, τ is a shifting time variable, and ω is the angular frequency. Here, a discrete STFT that provides identify and collect the frequency anomalies in the time domain was applied to obtain a time-frequency map of the TEC variation. The Gaussian window was also used as the window function g(t) (Harris, 1978).

$$g(t) = e^{-0.5\left(\alpha \frac{t}{(N-1)/2}\right)^2} \quad (12)$$

where N is the length of the window, and α could be termed as a frequency parameter. The width of the window is inversely related to the value of width factor (α), and the α parameter, ~~which~~ controls the frequency resolution at both extremities~~, was taken as 0.005 in this study~~. When α value increases, the window becomes narrower, so the selected α parameter gives relatively accurate resolution in the frequency domain (see Fig.1). Since it provided the best resolution, the α was chosen as 0.005 for this study.

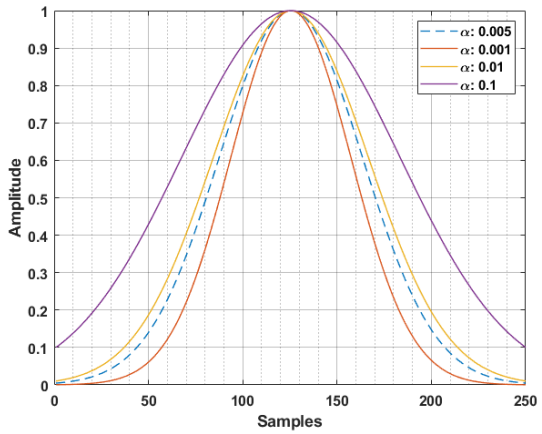

Figure 2. Gaussian windows functions according to α parameter.

A well-known anomaly detection method (running median) for seismoionospheric studies was used to validate STFT results. This method is based on distribution moments median (M) and standard deviation (σ). In our analysis, the median of TEC values in the previous 15 days was calculated to find the divergence from the observed TEC on the 16th day. The lower (LB) and upper (UB) bounds were calculated by Eq.13-14 to assign the level of the divergence.

$$LB = M - 2\sigma \quad (13)$$

$$UB = M + 2\sigma \quad (14)$$

When observed TEC of the 16th day is exceeded UB or LB, the positive or negative abnormal TEC signal is approved, respectively. The observed TEC between the UB and LB indicates no abnormal condition in the ionosphere. Assuming TECs are in a normal distribution with mean μ and standard deviation σ, the divergence of 2σ declare that ionospheric phases are detected with a confidence level of about %95.

The percentage of divergence degree of TEC (DTEC) was also calculated by the deviation from median values in GNSS TEC analysis. Since DTEC provides the relative TEC, it is more successful in detecting abnormalities at dusk when TEC values are lower.

$$\mathrm{DTEC} = [\mathrm{TEC}_{\mathrm{observed}} - \mathrm{TEC}_{\mathrm{median}}] \times 100/\mathrm{TEC}_{\mathrm{median}} \quad (15)$$

3 Results

3.1 Space Weather Before the Earthquake

The space weather indices Kp, Dst, F10.7, IMF Bz, Ey, and V_{SW} were cross-checked with TEC times series to reveal the effects of space weather on TEC disturbances. The indices obtained from the OMNI website (https://omniweb.gsfc.nasa.gov/form/dx1.html). The time series of the indices with 15 days before the earthquake were given in Fig. 3.

In Fig. 3a, IMF Bz~~,~~ and Ey indices have some fluctuations on 1-2 November ~~October~~ and 7-11 November~~October~~. These two indices remained calm on other days. In Fig. 3b, the V_{SW} index increased rapidly from 300 km/s to 650 km/s on November ~~October~~ 7. On the same day, the Dst index also decreased from +30 nT to -70 nT (see Fig. 3c). In both indices indicate~~s~~ a moderate magnetic storm (G2 level, Kp=6) on November 7~~occurred on the 7th of October~~. On the other days, it was determined that the indices values were at levels where atmospheric conditions to be considered calm. In Fig 3d, F10.7 and Kp indices were shown. F10.7 values continue to be quiet (<80 sfu) along 15 days before the earthquake. The index ranges from 65-75 sfu. Kp values indicate the disturbed magnetic condition between 7-11 November~~October~~, whereas other days have no magnetic activity values. Fig. 3 suggests that the moderate magnetic storm that occurred five days before the earthquake was capable until the one days before the earthquake. The fluctuations in IMF Bz and Ey indices on 1-2 November ~~October~~ were not seen in other indices. The other days are quite calm in terms of space weather.

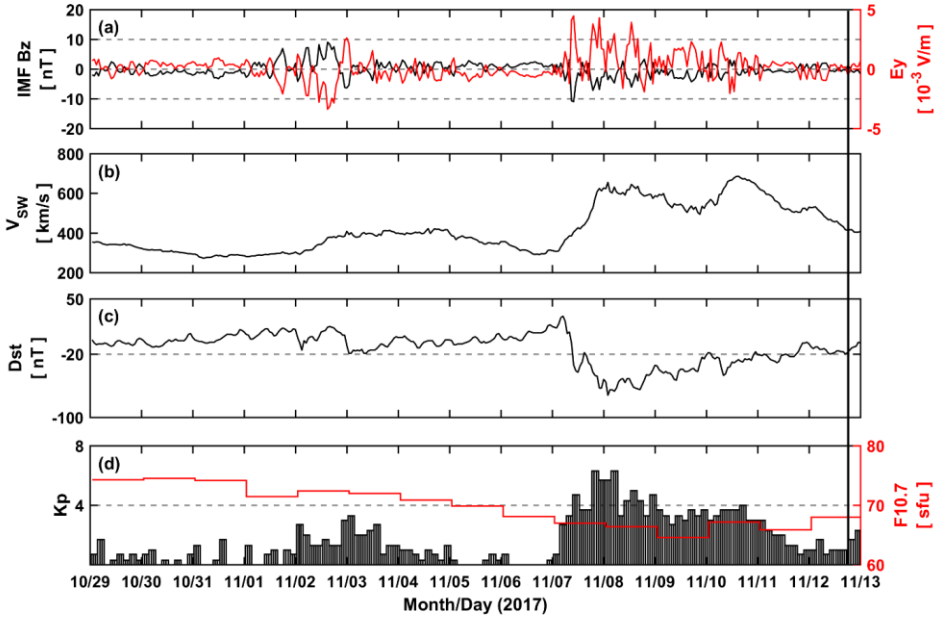

Figure 3. (a) IMF Bz and Ey (b) W_{SW} (c) Dst (d) Kp and F10.7 indices before 15 days of the earthquake. The vertical black line indicates the earthquake time.

3.2 Temporal and Spectral TEC Variation of GNSS Observations

TEC values over the epicenter location (34.911°N, 45.959°E) were obtained by interpolation from the vTEC values of the four grid points nearest to the epicenter in the GIMs to reveal ionospheric abnormalities in the zenith of the epicenter. The anomalies were detected by the running median method based on median and ±2 standard deviations. In Fig. 4, TEC values of CODE GIMs over the epicenter, positive/negative

anomalies, and Dst values were shown from October 14 to December 13, 2017. Fig. 4 showed that non-storm related abnormalities were observed only on 3-4 November as 1-3 TECU for 60 days, including 30 days before and after the earthquake.

In Fig. 5, GNSS based TEC time series of seven IGS stations named as ankr, aruc, bshm, isba, tehn, lroc, and lhaz were demonstrated. To better understand the earthquake-induced anomalies, lroc and lhaz stations have been chosen outside the EPA, further away from the epicenter. In the TEC calculation process, the satellite and receiver DCBs were obtained from IONEX files of CODE. The height of the single-layer was selected as 450 km and the elevation cut-off angle of 30° is taken. The sampling rate of TECs is 30 seconds. The results showed that positive anomalies were detected on November 3-4, 2017, with 1-3 TECU in five stations inside the EPA. No apparent anomaly was detected at two stations outside the EPA at these dates. Some positive/negative anomalies were also determined on November 7-12 in all stations. Negative anomalies range from 1-5 TECU. Especially, 15 TECU positive anomalies were observed at the lroc station on 7 November. These anomalies should be related to the moderate magnetic storm on 7-8 November.

~~In Fig. 4a observed and median TEC, upper/lower bounds were shown from 29 October to November 12, 2017. The anomalies were shown in Fig. 4b. There were 1-2 TECU positive anomalies on November 3-4 and some small positive/negative anomalies 1-6 days before the earthquake.~~

~~In Fig.5, the GNSS based TEC time series of ANKR, ARUC, BSHM, ISBA, and TEHN were demonstrated. The sampling rate of TEC data is 30 seconds. The stations were selected within the earthquake preparation area to reveal the earthquake-induced TEC fluctuations on TEC variation. The results showed that positive anomalies were detected on November 3-4, 2017, with 1-4 TECU in all stations. Some positive/negative anomalies were also determined on November 7-12. These anomalies should be related to the moderate magnetic storm that started on 7 November (the main phase of the storm occurred on 8 November).~~

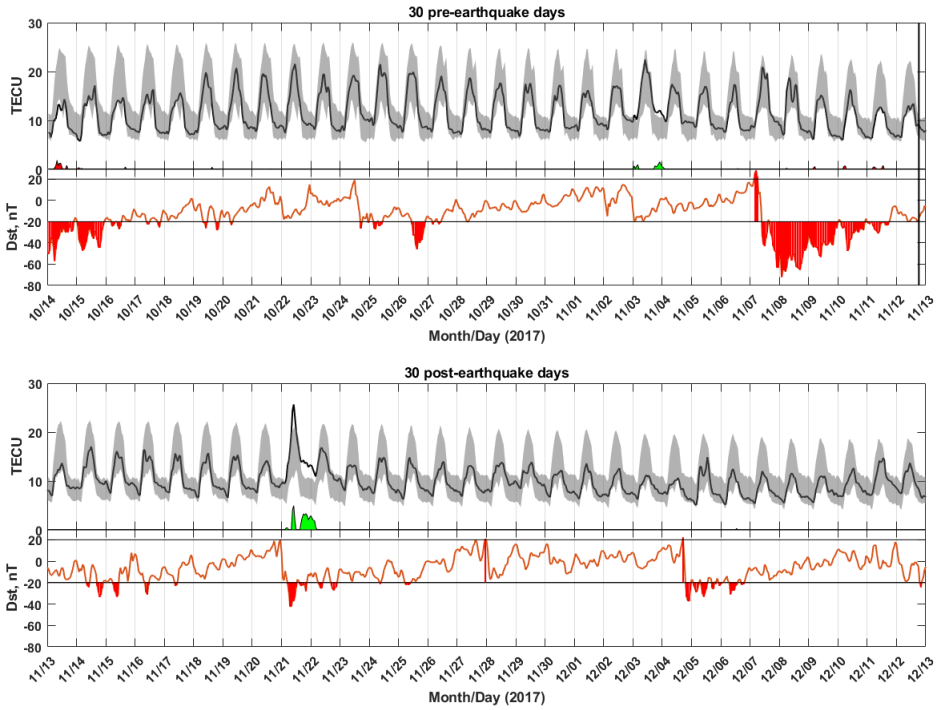

Figure 4. TEC values of CODE GIMs over the epicenter, positive/negative anomalies and Dst values during 30 pre- and post-earthquakes days. The vertical black line indicates the earthquake time.

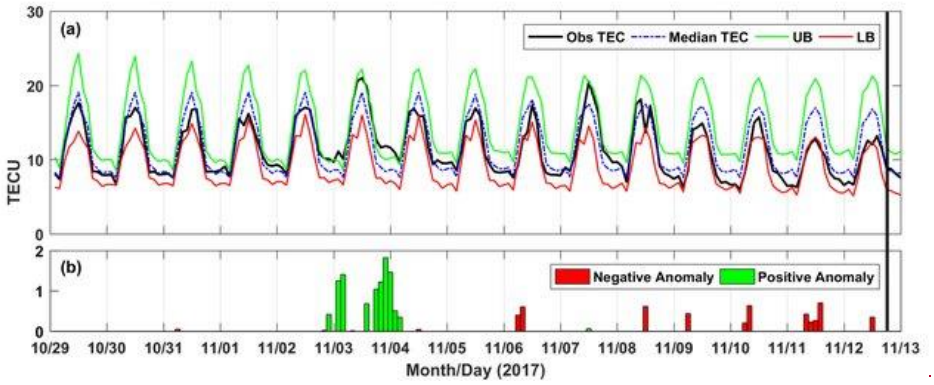

~~**Figure 4.** (a) TEC values of CODE GIMs over the epicenter (b) positive and negative anomalies. The vertical black line indicates the earthquake time.~~

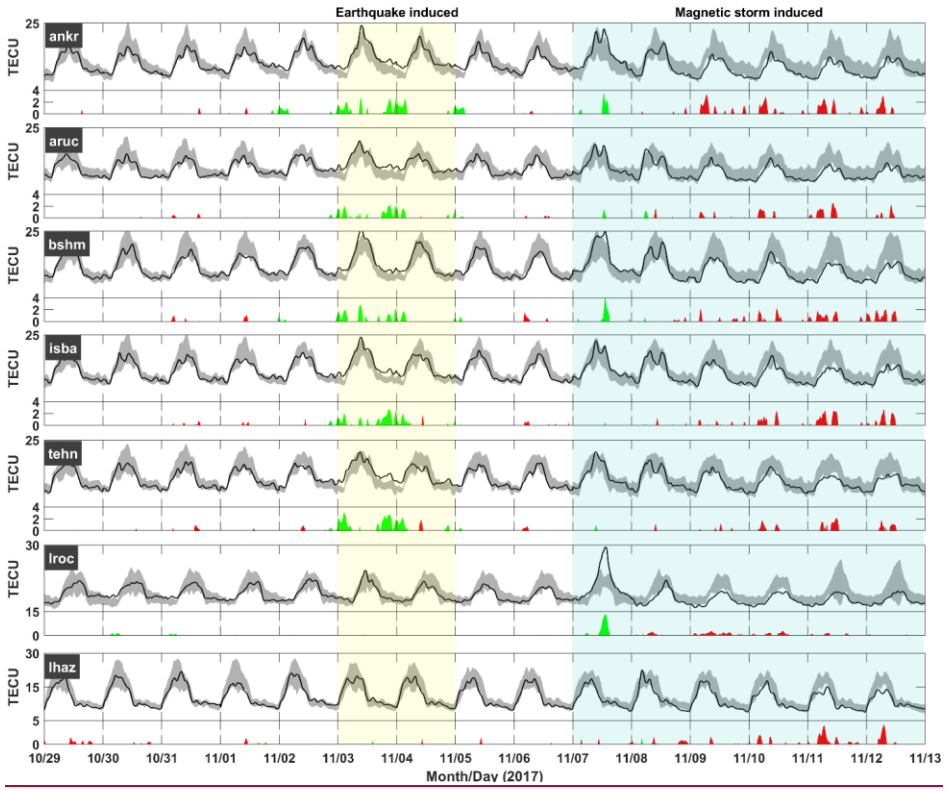

Figure 5. GNSS TEC variation of seven IGS stations. The solid black lines indicate TEC values of the stations, and the gray areas demonstrate M ± 2σ. The positive and negative anomalies were shown by green/red areas, respectively. The transparent yellow area indicates earthquake-induced and the transparent cyan area indicates magnetic storm-induced time intervals.

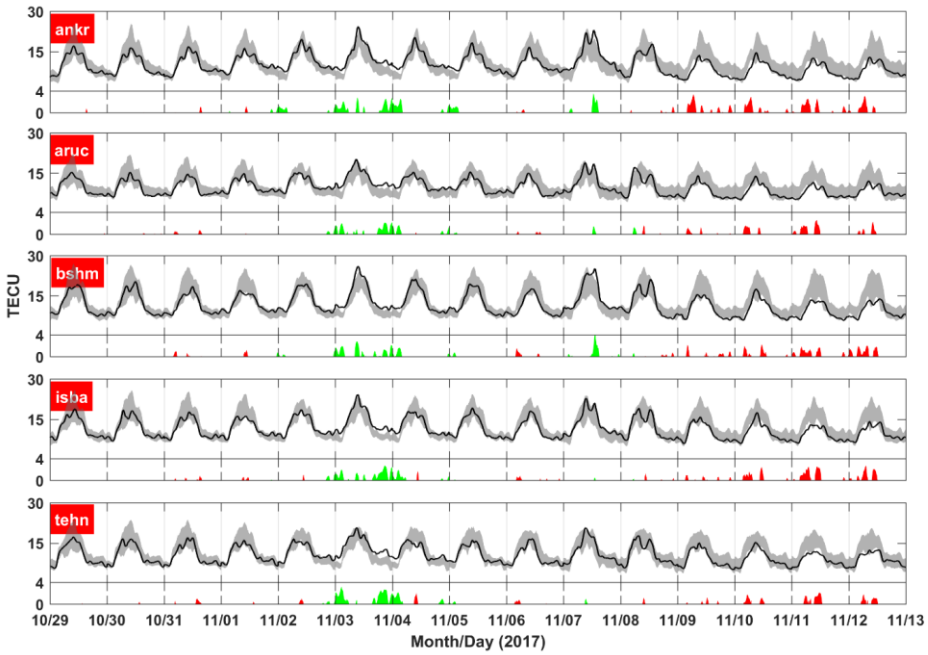

~~Figure 5.~~ ~~GNSS TEC variation of the five IGS stations where locate in the earthquake preparation area. The solid black lines indicate TEC values of stations, and the gray areas demonstrate M ± 2σ. The positive and negative anomalies were shown by green/red areas, respectively.~~

In Fig. 6, DTEC data of five IGS stations inside the EPA are given. DTEC reveals the relative change of observed TEC values to the median TEC values. The ionosphere has a significant day-to-day variability due to thermospheric dynamics even though quiet space weather. The diurnal TEC variation related to the lower atmosphere usually does not exceed ±30% according to the background TEC data (Forbes et al., 2000; Mendillo et al., 2002). In Fig. 6, we showed the ±30% limits~~the 30% limit~~ in the green area. Accordingly, DTEC values remaining in the green space can be accepted as the changes due to the daily day-to-day variability of the ionosphere. It was observed that the 30% limit was exceeded in the positive direction on November 2-5 and 7, in the negative direction between 8-12 November. The highest positive DTEC was detected on November 4 with + 62.5% and the lowest DTEC on November 9 with -43% at the ANKR station. Fig. 6 also indicated that the ± 30% limits of DTEC variation are consistent with the no-abnormal condition of the running median method (see Fig. 5).

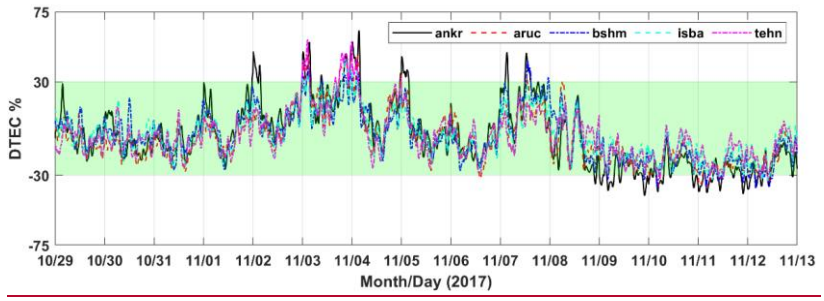

Figure 6. DTEC values of five IGS stations inside the EPA.

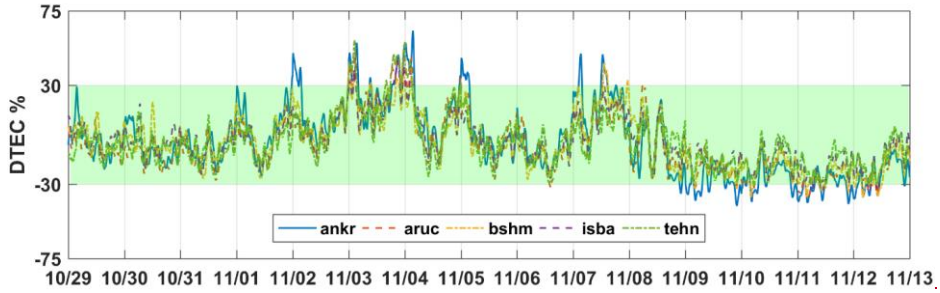

~~**Figure 6.** DTEC values of five IGS stations.~~

The STFT method was applied as a spectral analysis of GNSS based TEC data of five IGS stations inside the EPA with a 30-second sample rate. The method provides TEC anomalies both in the time and frequency domains. The amplitude value ranges from 0 to 30 TECU. The STFT results are shown in Fig. 7. At the ANKR station, high amplitude values are seen from November 2 to November 5 and November 7. The highest amplitude value of about 30 TECU was seen on November 3. At the ARUC station, high amplitudes were seen all day on November 3. This station has a relatively smaller amplitude (~24 TECU) value than the other stations. At the BSHM station, high amplitudes are seen on November 3 and 7. In this station, the highest amplitude value of 29.5 TECU was seen on November 7. At the ISBA and TEHN stations, the high amplitudes were recognized on November 3. The highest amplitudes are between 27-30 TECU. In all stations, the largest variations of the TEC anomalies correspond to smaller frequencies ($\leq 0.5 \times 10^{-5}$ Hz), and the maximum amplitudes are between 25 and 30 TECU. ~~The STFT analysis had a high amplitude on the days of anomalies, which is defined in the running median process. Therefore, the results of STFT are well correlated with classical methods. The fact that the STFT method reveals TEC anomalies without any background value is the strength of the method versus classical methods.~~

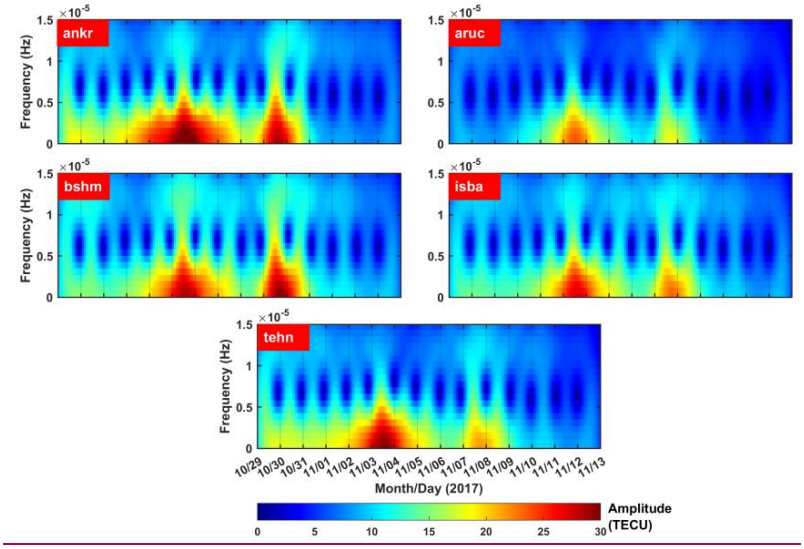

Figure 7. STFT analysis of GNSS TEC data of five IGS stations inside the EPA.

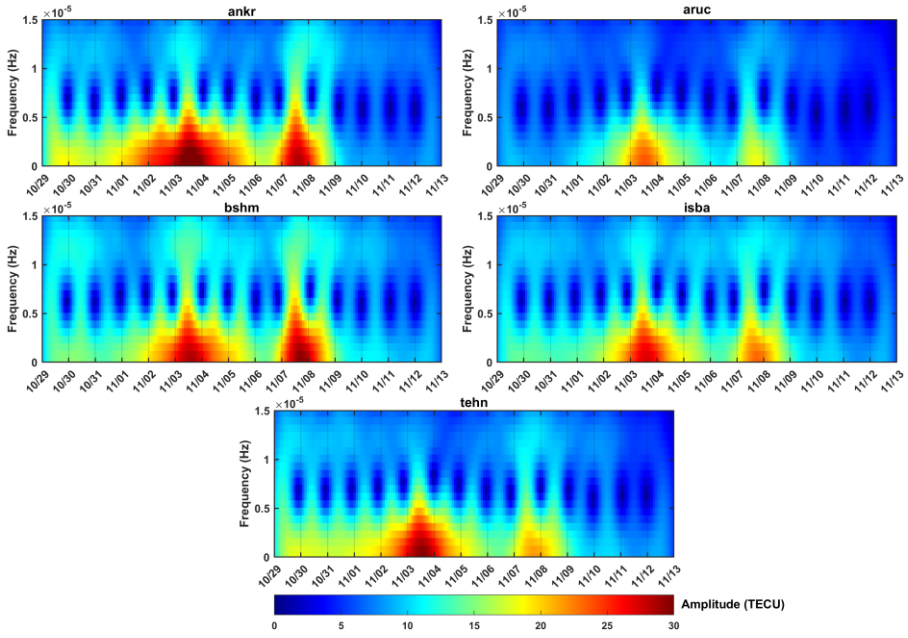

300

~~**Figure 7.** STFT analysis of GNSS TEC data of five IGS stations. The x-axis shows pre-earthquake days.~~The STFT analysis had a high amplitude on the days of anomalies, which is defined in the running median method (see Fig. 5). Therefore, the results of STFT are well-correlated with classical methods. The fact that the STFT method reveals TEC anomalies without any background value is the strength of the method versus classical methods.

3.3 Spatial Analysis of Abnormal Periods of TEC Variation

The remarkable abnormal days (3, 4, 7, and 8 November) detected in the temporal and spectral analysis were spatially investigated by anomaly maps, which are created with CODE GIM data. These anomaly maps bounded by 60^0 N-60^0 S latitudes, 180^0 W-180^0 E longitudes, and have a temporal resolution of 2-hours. In maps, the epicenter of the earthquake is shown with ~~in~~ a purple star~~circle~~. The TEC anomalies in the anomaly maps were detected by the running median method based on $M \pm 2\sigma$. In Fig. 8, the anomalies range ±5 TECU ~~between -5 and +7 TECU~~ on November 3-4. Fig. 8 showed that anomaly areas were locally distributed and a notable anomaly area concentrated near the earthquake epicenter. This area located toward the Northeast side of the epicenter with 1-3~~2 5~~ TECU from 14:00 UTC to 02:00 UTC on November 3-4. An anomaly area also located on the Southeast side of the epicenter with ~~6 7~~ 5 TECU between 04:00 and 06:00 UTC on November 4. These anomalies are interesting because no other anomaly region is seen in a large area, and it is located only in close areas to the epicenter. In Fig. 9, the anomalies range between ±10 TECU ~~-6 and +14 TECU~~ on November 7-8. The only remarkable detail here is that the anomalies are distributed globally, as opposed to Fig. 8. The changes detected in the relevant days mostly point to an ionospheric variation caused by a magnetic storm.

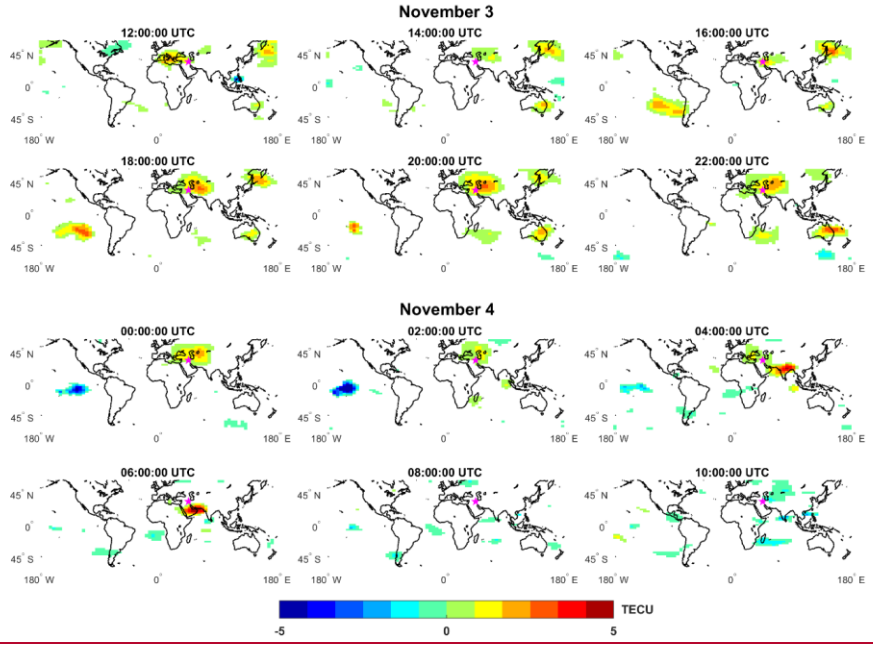

Figure 8. The anomaly maps on November 3-4, 2017.

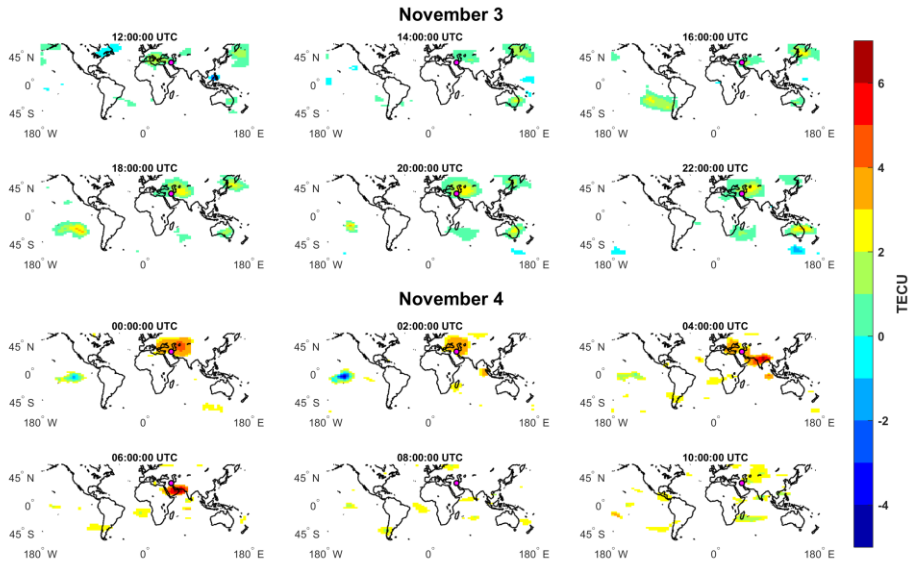

~~**Figure 8.** The anomaly maps on November 3-4, 2017.~~

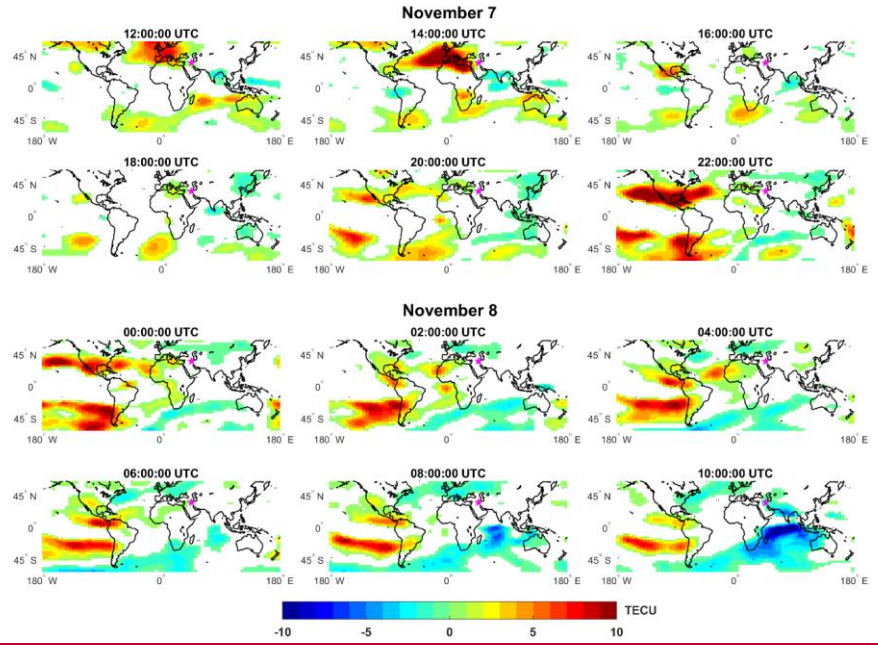

Figure 9. The anomaly maps on November 7-8, 2017.

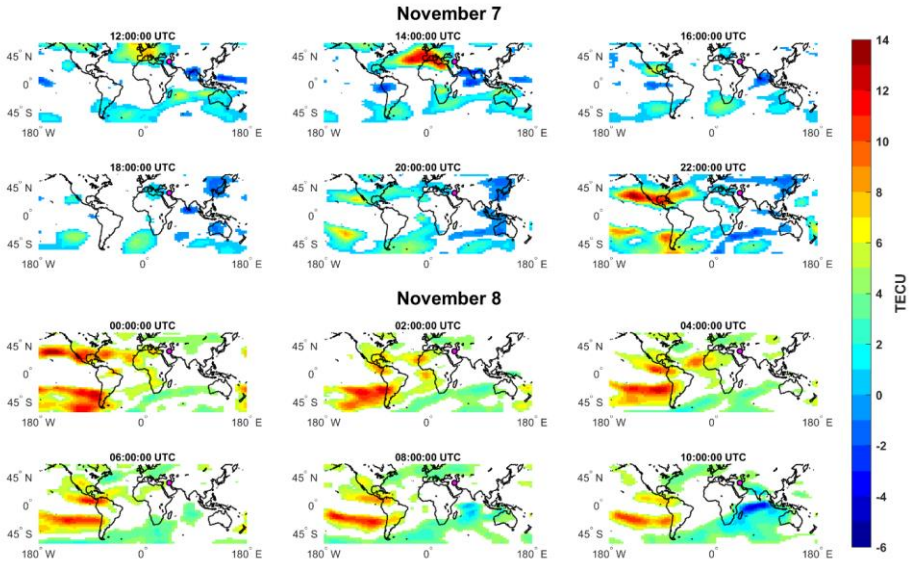

~~**Figure 9.** The anomaly maps on November 7-8, 2017.~~

It is reasonable to argue that anomalies that occur in the nighttime in the period of calm space weather may be related to the earthquake or other phonemes because the solar penetration towards the ionosphere reduces in the night. Therefore, the detected anomalies between 18:00 UTC (21:00 LT) and 02:00 UTC (05:00 LT) on November 3-4 should be the precursor of the Iran-Iraq border earthquake due to dusk time, quiet space weather and local distribution.

3.4. The Prompt Penetration Electric Fields (PPEFs) Variation in Abnormal Days

The PPEFs is the prompt reaction of the equatorial zonal electric field to solar wind alteration, which is the component of the interplanetary electric field (IEF) and the equatorial zonal electric field (Manoj et al., 2008). The penetration part of PPEFs (green line in Fig. 10) is calculated by the interplanetary data which is provided by the OMNI web site. Also, the quiet (climatological) part of PPEFs (violet line in Fig. 10) is related to the 81-day moving average of F10.7 cm solar flux (Manoj and Maus, 2012).

Fig. 10 showed the prompt penetration electric fields (PPEFs) at 46^0 E longitude (geographical longitude of the epicenter) on 3-4 November and 7-8 November. The PPEFs are observable in the ionosphere immediately after being transported to the magnetosphere by the solar wind (Tsurutani et al., 2008). The PPEFs also occur during the negative values of IMF Bz (Astafyeva et al., 2016). Fig. 3 indicated an increase of the solar wind from 300 km/s to 650 km/s, and the IMF Bz decreased to negative values as about -10 nT. Accordingly, fluctuations in PPEF variation are observed between 06:00 UTC and 02:00 UTC on November 7-8 (see Fig. 10b). Many studies have reported that PPEFs cause positive and negative phases in the ionosphere during magnetic storms (Basu et al., 2007; Tsurutani et al., 2008; Mannucci et al., 2009; Lu et al., 2012; Astafyeva et al., 2016). Fig 10b indicated that the moderate magnetic storm caused the positive and negative anomalies in the ionosphere along with the change in PPEF values on 7-8 November. On the contrary, no significant difference in PPEF values was observed in Fig. 10a. These PPEFs values indicated that a magnetic storm or solar wind could not affect the TEC variation on 3-4 November.

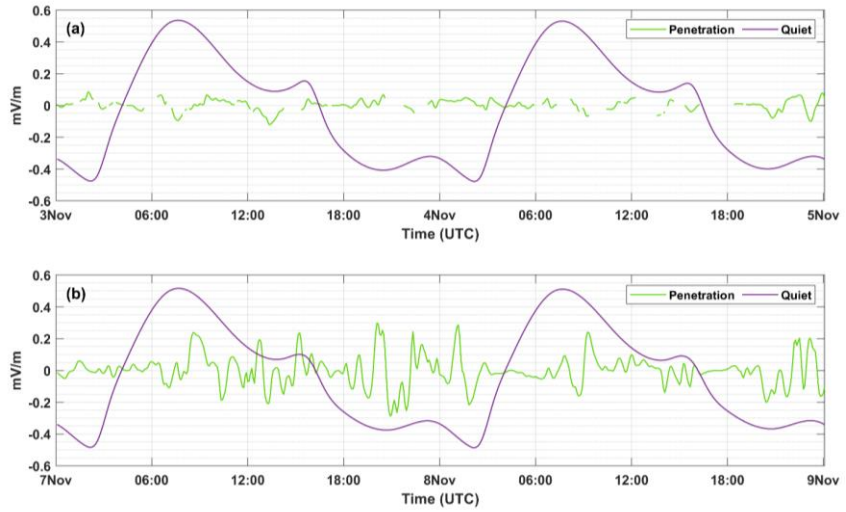

Figure 10. The prompt penetration electric fields at 46^0 E longitude (a) on November 3-4 (b) on November 7-8, 2017.

Biçimlendirilmiş: Girinti: İlk satır: 0 cm

4 Conclusion

The TEC data of CODE GIM and seven ~~five~~ IGS stations were analyzed to reveal the earthquake-induced ionospheric anomalies of the Mw 7.3 Iran-Iraq border earthquake. For this purpose, a classical method named as running median and STFT method were applied to the TEC time series from October 29 to November 13, 15 days before the earthquake. Only the CODE GIM time series were analyzed for 60 days, including 30 days before and after the earthquake. Thus, it has been revealed that the anomalies obtained are not a coincidence. Abnormalities are observed only on 3-4 November, when the Dst values represent quiet geomagnetic conditions (Dst > -20 nT). The running median process of TEC variation was shown considerable positive anomalies as 1-3~~4~~ TECU on November 3-4 both in the GIM and GNSS time series except for the TEC time series of the lroc and lhaz stations which locate outside the EPA.~~.~~ This value is outlined from the mean of a normal distribution with a width of two standard deviations that is defined as a 95% confidence level. These positive anomalies were also detected in the spectral analysis. The STFT method was used for spectral analysis. STFT is a powerful tool for processing a time series without any background values (mean, median, quiet days, etc.). Independence from background data minimizes the error sources of these data (other unexpected changes, main trends of the ionosphere such as annual, semi-annual, and seasonal). The results showed the power of the STFT method in the detection of TEC anomalies.

There are some positive/negative anomalies 1-6 days before the earthquake, but these anomalies should be caused by a moderate geomagnetic storm on November 7-8. A geomagnetic storm affects the ionosphere as a whole, producing more global variations of TEC compared to the localized phenomena of seismoionospheric coupling. In Fig. 9, the global TEC changes of the moderate magnetic storm ~~is~~ are seen.

On the contrary, the anomalies occurring on 3-4 November, which are thought to be caused by the earthquake, have local distribution, and are concentrated near the epicenter (see Fig. 8).

Fig. 10 showed the prompt penetration electric fields (PPEFs) at 46^0 E longitude (geographical longitude of the epicenter) on 3-4 November and 7-8 November. The PPEFs are observable in the ionosphere immediately after being transported to the magnetosphere by the solar wind (Tsurutani et al., 2008). The PPEFs also occur during the negative values of IMF Bz (Astafyeva et al., 2016). Fig. 3 indicated an increase of the solar wind from 300 km/s to 650 km/s, and the IMF Bz decreased to negative values as about -10 nT. Accordingly, fluctuations in PPEF variation are observed between 06:00 UTC and 02:00 UTC on November 7-8 (see Fig. 10b). Many studies have reported that PPEFs cause positive and negative phases in the ionosphere during magnetic storms (Basu et al., 2007; Tsurutani et al., 2008; Mannucci et al., 2009; Lu et al., 2012; Astafyeva et al., 2016). Fig 10b indicated that the moderate magnetic storm caused the positive and negative anomalies in the ionosphere along with the change in PPEF values on 7-8 November. On the contrary, no significant difference in PPEF values was observed in Fig. 10a. These PPEFs values indicated that a magnetic storm or solar wind could not affect the TEC variation on 3-4 November.

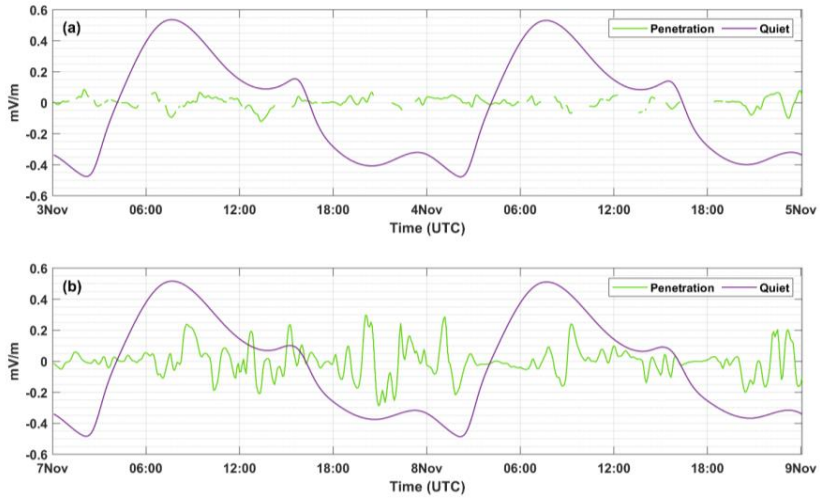

Figure 10. The prompt penetration electric fields at 46^0 E longitude (a) on November 3-4 (b) on November 7-8, 2017.

Although the space weather is rather quiet on 3-4 November, the DTEC values of the five IGS stations inside the EPA exceeded the ±30% limits 30% limit corresponding to the day-to-day variability of the ionospheric TEC and reached 65%. This value indicates remarkable positive ionospheric anomalies. It can be said that the positive anomalies 8-9 days before the earthquake should be associated with the Iraq-Iran border earthquake because they occurred in the close areas to the epicenter and dispersed in local rather than global. Also, the anomalies continued all day, detecting at all IGS stations inside the EPA which are near the epicenter.

This study showed the advantages of using different approaches to detect earthquake-related anomalies. Notably, it will be useful to prefer spectral analysis methods for the anomaly detection process as a new and promising approach in future studies.

Data availability. The RINEX files of the IGS stations are publicly available at the IGS website ftp://igs.ensg.ign.fr/pub/igs/data/, the IONEX files of CODE are publicly available at the NASA website ftp://cddis.gsfc.nasa.gov/gps/products/ionex/, and the space weather indices are publicly available at the OMNI website https://omniweb.gsfc.nasa.gov/form/dx1.html.

Author contributions. ES carried out the data analysis, prepared the plots, and interpreted the results. SI provided processed GIM based TEC time series. IS interpreted the storm-time effects on the ionosphere. ES prepared the manuscript with contributions from all authors.

Competing interests. The authors declare that they have no conflicts of interest.

References

Astafyeva, E., Zakharenkova, I., Alken, P. (2016). Prompt penetration electric fields and the extreme topside ionospheric response to the June 22–23, 2015 geomagnetic storm as seen by the Swarm constellation. Earth, Planets and Space, 68(1), 1-12.

Bagiya, M. S., Joshi, H. P., Iyer, K. N., Aggarwal, M., Ravindran, S., Pathan, B. M. (2009). TEC variations during low solar activity period (2005–2007) near the equatorial ionospheric anomaly crest region in India. Annales Geophysicae, 27(3), 1047-1057.

Basu, S., Basu, S., Rich, F. J., Groves, K. M., MacKenzie, E., Coker, C., ... Becker-Guedes, F. (2007). Response of the equatorial ionosphere at dusk to penetration electric fields during intense magnetic storms. Journal of Geophysical Research: Space Physics, 112(A8).

Burrus, C. S. (1995). Multiband least squares FIR filter design. IEEE transactions on signal processing, 43(2), 412-421.

~~Calais, E., Minster, J. B. (1995). GPS detection of ionospheric perturbations following the January 17, 1994, Northridge earthquake. Geophysical Research Letters, 22(9), 1045-1048.~~

Chou, M. Y., Lin, C. C., Yue, J., Tsai, H. F., Sun, Y. Y., Liu, J. Y., Chen, C. H. (2017). Concentric traveling ionosphere disturbances triggered by Super Typhoon Meranti (2016). Geophysical Research Letters, 44(3), 1219-1226.

Ciraolo, L., Azpilicueta, F., Brunini, C., Meza, A., Radicella, S. M. (2007). Calibration errors on experimental slant total electron content (TEC) determined with GPS. Journal of Geodesy, 81(2), 111-120.

Çepni, M. S., Şentürk, E. (2016). Geometric quality term for station-based total electron content estimation. Annals of geophysics, 59(1), A0107.

Dach, R., Schaer, S., Arnold, D., Kalarus, M. S., Prange, L., Stebler, P., Villiger, A., Jäggi, A. (2020). CODE final product series for the IGS. Published by Astronomical Institute, University of Bern. DOI: 10.7892/boris.75876.4.

~~Davies, K., Baker, D. M. (1965). Ionospheric effects observed around the time of the Alaskan earthquake of March 28, 1964. Journal of Geophysical Research, 70(9), 2251-2253.~~

Dautermann, T., Calais, E., Lognonné, P., Mattioli, G. S. (2009). Lithosphere-atmosphere-ionosphere coupling after the 2003 explosive eruption of the Soufriere Hills Volcano, Montserrat. Geophysical Journal International, 179(3), 1537-1546.

Dobrovolsky, I.P., Zubkov, S.I., Miachkin, V.I. (1979). Estimation of the size of earthquake preparation zones. Pure Appl. Geophys. 117, 1025-1044.

Forbes, J. M., Palo, S. E., Zhang, X. (2000). Variability of the ionosphere. Journal of Atmospheric and Solar-Terrestrial Physics, 62(8), 685-693.

Freund, F. T., Takeuchi, A., Lau, B. W. (2006). Electric Currents Streaming Out of Stressed Igneous Rocks–A Step Towards Understanding Pre-Earthquake Low Frequency EM Emissions. Physics and Chemistry of the Earth, Parts A/B/C, 31(4-9), 389-396.

Freund, F. T., Kulahci, I. G., Cyr, G., Ling, J., Winnick, M., Tregloan-Reed, J., Freund, M. M. (2009). Air Ionization at Rock Surfaces and Pre-earthquake Signals. Journal of Atmospheric and Solar-Terrestrial Physics, 71(17), 1824-1834.

Freund, F. T. (2011). Pre-Earthquake Signals: Underlying Physical Processes. Journal of Asian Earth Sciences, 41(4-5), 383-400.

Fuying, Z., Yun, W., Ningbo, F. (2011). Application of Kalman filter in detecting pre-earthquake ionospheric TEC anomaly. Geodesy and Geodynamics, 2(2), 43-47.

Gabor, D. (1946). Theory of communication. Part 1: The analysis of information. Journal of the Institution of Electrical Engineers-Part III: Radio and Communication Engineering, 93(26), 429-441.

~~Gokhberg, M. B. (1983). Strong acoustic wave action. In ESA Special Publication, 195, 99-110.~~

Harris, F. J. (1978). On the use of windows for harmonic analysis with the discrete Fourier transform. Proceedings of the IEEE, 66(1), 51-83.

Hein, W. Z., Goto, Y., Kasahara, Y. (2016). Estimation method of ionospheric TEC distribution using single frequency measurements of GPS signals. International Journal of Advanced Computer Science and Applications, 7(12), 1-6.

Hofmann-Wellenhof, B., Lichtenegger, H., Collins, J. (1992). Global Positioning System Theory and Practice. Springer-Verlag Wien, New York.

Ke, F., Wang, J., Tu, M., Wang, X., Wang, X., Zhao, X., Deng, J. (2018). Enhancing reliability of seismo-ionospheric anomaly detection with the linear correlation between total electron content and the solar activity index F10. 7: Nepal earthquake 2015. Journal of Geodynamics, 121, 88-95.

Leonard, R. S., Barnes, R. A. (1965). Observation of ionospheric disturbances following the Alaska earthquake. Journal of Geophysical Research, 70(5), 1250-1253.

Li, M., Zhang, B., Yuan, Y., Zhao, C. (2019). Single-frequency precise point positioning (PPP) for retrieving ionospheric TEC from BDS B1 data. GPS Solutions, 23(1), 18.

Lin, C. C., Shen, M. H., Chou, M. Y., Chen, C. H., Yue, J., Chen, P. C., Matsumura, M. (2017). Concentric traveling ionospheric disturbances triggered by the launch of a SpaceX Falcon 9 rocket. Geophysical Research Letters, 44(15), 7578-7586.

Liu, J. Y., Chen, Y. I., Pulinets, S. A., Tsai, Y. B., Chuo, Y. J. (2000). Seismo-ionospheric signatures prior to M≥ 6.0 Taiwan earthquakes. Geophysical Research Letters, 27(19), 3113-3116.

Liu, J. Y., Chen, Y. I., Chen, C. H., Hattori, K. (2010). Temporal and spatial precursors in the ionospheric global positioning system (GPS) total electron content observed before the 26 December 2004 M9.3 Sumatra–Andaman Earthquake. Journal of Geophysical Research: Space Physics, 115(A9).

Liu, J. Y., Chuo, Y. J., Shan, S. J., Tsai, Y. B., Chen, Y. I., Pulinets, S. A., Yu, S. B. (2004). Pre-earthquake ionospheric anomalies registered by continuous GPS TEC measurements. Annales Geophysicae, 22(5), 1585-1593.

Lu, G., Goncharenko, L., Nicolls, M. J., Maute, A., Coster, A., Paxton, L. J. (2012). Ionospheric and thermospheric variations associated with prompt penetration electric fields. Journal of Geophysical Research: Space Physics, 117(A8).

Mannucci, A. J., Tsurutani, B. T., Kelley, M. C., Iijima, B. A., Komjathy, A. (2009). Local time dependence of the prompt ionospheric response for the 7, 9, and 10 November 2004 superstorms. Journal of Geophysical Research: Space Physics, 114(A10).

Manoj, C., Maus, S., Lühr, H., Alken, P. (2008). Penetration characteristics of the interplanetary electric field to the daytime equatorial ionosphere. Journal of Geophysical Research: Space Physics, 113(A12).

Manoj, C., Maus, S. (2012). A real-time forecast service for the ionospheric equatorial zonal electric field. Space Weather, 10(9), 1-9.

Mendillo, M., Rishbeth, H., Roble, R. G., Wroten, J. (2002). Modelling F2-layer seasonal trends and day-to-day variability driven by coupling with the lower atmosphere. Journal of Atmospheric and Solar-Terrestrial Physics, 64(18), 1911-1931.

Molchanov, O. A., Kopytenko, Y. A., Voronov, P. M., Kopytenko, E. A., Matiashvili, T. G., Fraser-Smith, A. C., Bernardi, A. (1992). Results of ULF magnetic field measurements near the epicenters of the Spitak (Ms= 6.9) and Loma Prieta (Ms= 7.1) earthquakes: Comparative analysis. Geophysical Research Letters, 19(14), 1495-1498.

Namgaladze, A., Klimenko, M. V. V., Klimenko, V., Zakharenkova, I. E. (2009). Physical Mechanism and Mathematical Modeling of Earthquake Ionospheric Precursors Registered in Total Electron Content. Geomagnetism and Aeronomy, 49(2), 252-262.

~~Pulinets, S. A. (1998). Strong earthquake prediction possibility with the help of topside sounding from satellites. Advances in Space Research, 21(3), 455-458.~~

Pulinets, S. A., Ouzounov, D., Karelin, A. V., Boyarchuk, K. A., Pokhmelnykh, L. A. (2006). The Physical Nature of Thermal Anomalies Observed before Strong Earthquakes. Physics and Chemistry of the Earth, 31(4), 143-153.

Occhipinti, G., Rolland, L., Lognonné, P., Watada, S. (2013). From Sumatra 2004 to Tohoku-Oki 2011: The systematic GPS detection of the ionospheric signature induced by tsunamigenic earthquakes. Journal of Geophysical Research: Space Physics, 118(6), 3626-3636.

Schaer, S., Gurtner, W., Feltens, J. (1998). IONEX: The ionosphere map exchange format version 1. In Proceedings of the IGS AC workshop, Darmstadt, Germany (Vol. 9, No. 11).

Schaer, S. (1999). Mapping and Predicting the Earth's Ionosphere Using the Global Positioning System. PhD Thesis. University of Bern, Bern, Switzerland.

Şentürk, E., Livaoğlu, H., Çepni, M. S. (2019). A Comprehensive Analysis of Ionospheric Anomalies before the Mw 7.1 Van Earthquake on 23 October 2011. The Journal of Navigation, 72(3), 702-720.

Tariq, M. A., Shah, M., Hernández-Pajares, M., Iqbal, T. (2019). Pre-earthquake ionospheric anomalies before three major earthquakes by GPS-TEC and GIM-TEC data during 2015-2017. Advances in Space Research, 63(7), 2088-2099.

Toutain, J. P., Baubron, J. C. (1998). Gas Geochemistry and Seismotectonics: A Review. Tectonophysics, 304(1), 1-27.

Tsurutani, B. T., Verkhoglyadova, O. P., Mannucci, A. J., Saito, A., Araki, T., Yumoto, K., ... & McCreadie, H. (2008). Prompt penetration electric fields (PPEFs) and their ionospheric effects during the great magnetic storm of 30–31 October 2003. Journal of Geophysical Research: Space Physics, 113(A5).

Ulukavak, M., Yalcinkaya, M. (2017). Precursor analysis of ionospheric GPS-TEC variations before the 2010 M 7.2 Baja California earthquake. Geomatics, Natural Hazards and Risk, 8(2), 295-308.

U.S. Geological Survey (2017). Earthquake Lists, Maps, and Statistics, accessed March 28, 2019 at URL https://earthquake.usgs.gov/earthquakes/browse/

Yan, X., Yu, T., Shan, X., Xia, C. (2017). Ionospheric TEC disturbance study over seismically region in China. Advances in Space Research, 60(12), 2822-2835.

Yildirim, O., Inyurt, S., Mekik, C. (2016). Review of variations in Mw< 7 earthquake motions on position and TEC (Mw= 6.5 Aegean Sea earthquake sample). Nat. Hazards Earth Syst. Sci, 16, 543-557.

RESPONSE TO REVIEWER#1

SPECIFIC COMMENTS (MAJOR COMMENTS)

1. As of my awareness, CODE provides interpolated (spherical harmonic fitted) TEC maps (please provide a citation at L105). This may result in biases generated by data interpolation. What accuracy is expected for the derived vTEC values over the epicenter based on CODE TEC maps? Why authors found it is necessary to analyze interpolated CODE maps, instead of just considering 5 available stations (Table 1) and calculating TEC over epicentral position with them? Also, does CODE use the same IGS stations in the considered region to produce vTEC maps? If so, authors analyze the same data twice (e.g., Figure 4 and 5). Please, clarify which stations in the considered region are used by CODE. Again, how good "anomaly maps" are for the estimation of absolute deviations (as they also based on CODE GIM interpolated data)? Were they cross-checked with vTEC over the epicenter calculated based on 5 stations? Do values agree?

- The main purpose of using GIM TECs was to validate the calculated GNSS TECs with a reliable data. Now, we have expanded this validation even further (the analyzes and results in below are not included in the article. It was only carried out in response to your question.)
- We estimated the CODE GIM vTEC values at the location of the GNSS stations (ankr, aruc, bshm, isba and tehn) similar to the vTECs of the epicenter. The RMSE and Bias values are seen in the Fig.1. RMSE values range between 0.52-0.68 TECU and Bias values range between 0.01-0.44 TECU.
- The RMSE and Bias values indicated that GIM vTEC values of CODE compatible with GNSS TECs of IGS stations. These values also prove the accuracy of "anomaly maps".
- A citation added for CODE GIM at L100.

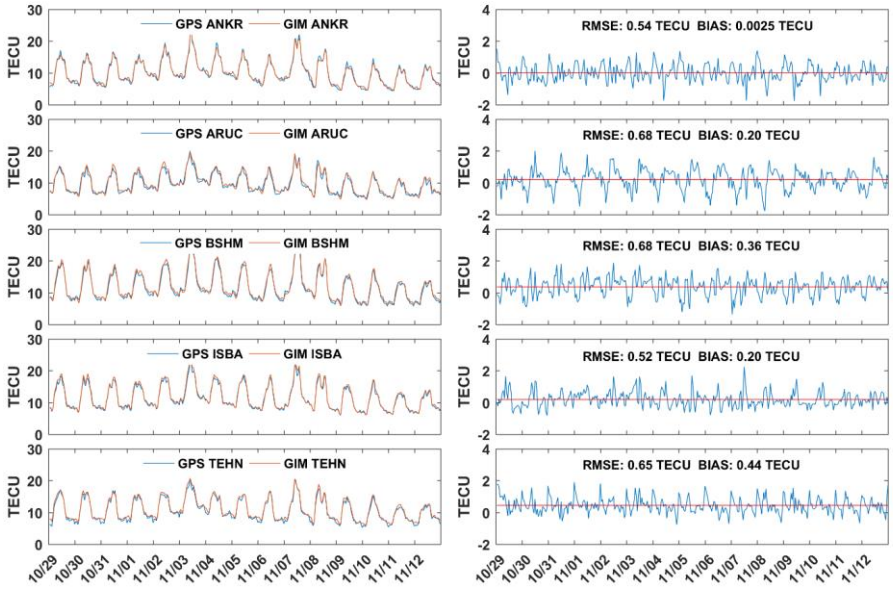

Figure 1 GNSS TECs and GIM vTECs at the location of IGS stations (left panel), differences between GNSS and GIM, RMSE and Bias values (right panel).

2. Authors introduce satellite and receiver biases (eq. 2), but do not indicate if these biases were corrected. It is not clear what methodology is used for the correction of these biases and what errors are expected for the determination of vTEC. The analysis and incorporation of these biases is an important factor while discussing the variations of absolute vTEC and I believe this should be clarified in the text.

- We used the TEC time series of IGS station so DCBs were obtained from daily IONEX files.
- We added a new sentence in L130. *"The DCBs of satellites and receivers are available in the daily IONEX files for IGS stations, but receiver DCBs of no-IGS stations must be calculated in the TEC calculation process."*

3. Authors provide the equation for the calculation of TEC averaged from all satellites (eq. 7). However, it is not clear if all Ionospheric Pierce Points (IPP) for used observations were over the earthquake preparation area (determined as 1380 km). If authors carry out the selection of TEC observations outside this area, it seems possible that found anomalies results from the area outside of it. For eq. 6, it is not clear what ionospheric shell height is used for the calculation of vTEC. Also, it is not clear what elevation angle cut-off is used for vTEC observations based on eq. 7.

- In the vTEC weighting process of obtaining TEC values of a station zenith, the VTEC value of a satellite with a low elevation angle already has low weight. TEC values are generally calculated as the VTEC value of a satellite with an elevation angle between 70^0-90^0 (these IPPs are already very close to the station). Also, the earthquake preparation area is an empirical value and it is not absolute.
- We added a new sentence in L220. *"In the TEC calculation process, the satellite and receiver DCBs were obtained from IONEX files of CODE. The height of the single-layer was selected as 450 km and the elevation cut-off angle of 30° is taken."*

4. In my opinion, authors use very narrow range of days and only prior to the earthquake (from 10/29 to 11/13). It is crucial to understand whether positive anomalies appear only before the earthquake or on a constant basis during quite times. Such analysis requires additional processing of data before and after the earthquake. I would consider range between -3/+3 months, along with the analysis of geomagnetic indexes and the use of the same stations over the same region.

- We revised the Fig.4 as below. In the new version of Fig. 4, the 30 pre- and post-earthquake days were analyzed with the same method in the previous version.
- We also revised texts in all manuscript related to the change in Fig. 4.
- In Fig.4 (Fig.2 in this file), it was seen that anomalies occurred only on 3-4 November for quiet Dst (Dst > -20) during 60 days. Also, GIM and GNSS TEC values are in good agreement as stated in Q1, so we did not perform the same analysis for GNSS data. GNSS time series includes 15 days before the earthquake as the previous version of the article.
- We added a new sentence in L310. *"Only the CODE GIM time series were analyzed for 60 days, including 30 days before and after the earthquake. Thus, it has been revealed that the anomalies obtained are not a coincidence. Abnormalities are observed only on 3-4 November, when the Dst values represent quiet geomagnetic conditions (Dst > -20 nT)."*

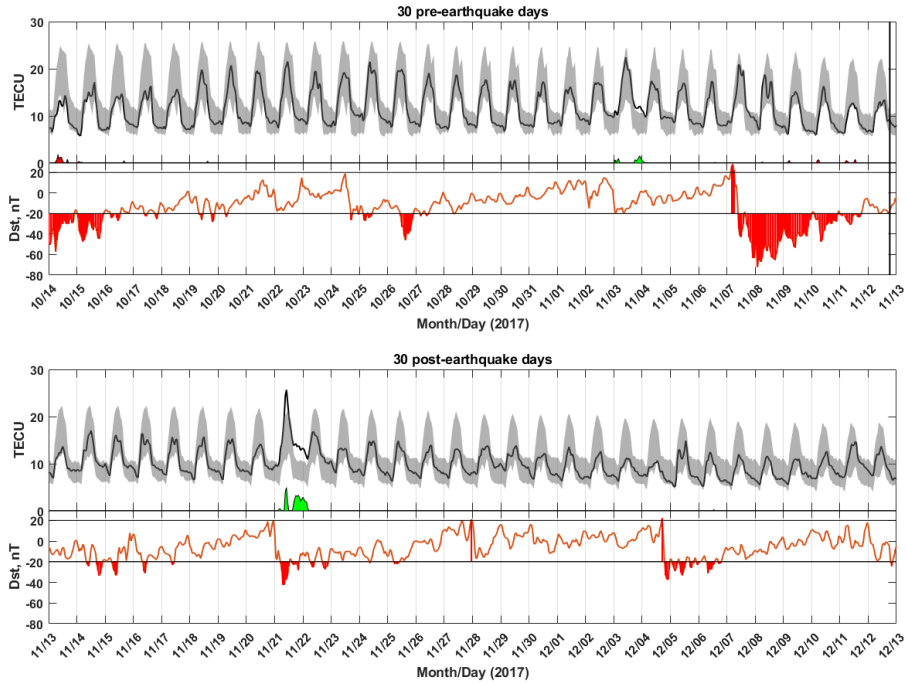

Figure 2 TEC values of CODE GIMs over the epicenter, positive/negative anomalies and Dst values during 30 pre- and post-earthquakes days.

5. Authors reference publications by Forbes et al., 2020 and Mendillo et al. 2002, but they do not explicitly mention that TEC observation variability cannot exceed 30%, incorporating possible satellite and instrumentation biases as well as integrated nature of TEC, IPP locations, recalculation of vTEC from sTEC etc. Also, Forbes et al., 2000 discuss "high frequency" variability of 25-35% under quite Kp index < 1, whereas (according to Figure 3), Kp index on 3rd and 4th of November seem to be higher than 1 (especially on 3rd of November, where Kp index approaches 4). Do authors expect the same ~25-35% variability for Kp index of 4?

- Please examine the anomalies in Fig. 5 and the situations exceeding ±30% in Fig. 6. You will notice the similarity. In Fig. 5, no-abnormal TEC conditions are determined with a 95% confidence level. DTEC values were within the 30% limit when GNSS TECs do not exceed upper or lower bounds. Here, the ±30% limit for DTECs represented quiet ionospheric conditions. However, I need to examine more data to reach a definitive conclusion about this. That's why I have cited some previous studies.
- In fact, it is important here not what Kp index values are, but whether TEC values represent abnormal conditions in the time series. The ±30% limit for DTEC is equivalent to the TEC value between the upper and lower limit (no-abnormal condition) in the running median method.
- We added a new sentence in L245. *"Fig. 6 also indicated that the ± 30% limits of DTEC variation are consistent with the no-abnormal condition of running median method (see Fig. 5)."*

TECHNICAL COMMENTS (MINOR COMMENTS)

1. Please, clarify the choice of the window for Gaussian function as 0.005. What period it corresponds?

- A value of 0.005 is a coefficient that controls the frequency resolution of the gauss window function. It is not related to the period. We used it because we provide the best resolution with this value.
- We added a new explanation in L170. *"Since it provided the best resolution, the α was chosen as 0.005 for this study."*

2. Consider using the same x-axis on all plots (e.g., on Figure 7, there are days prior to the earthquake, although on Figure 5 there are Month/Day). Also, authors may want to indicate periods instead of frequencies, as it is difficult to assess the period from ~10^-5 Hz).

- We revised the x-axis of Fig.7 as "Month/Day". The revised version of Fig. 7 is below.
- The y-axis in graphs indicate Fourier frequencies according to sampling rates of the TECs. So it is not necessary to convert them into periods.

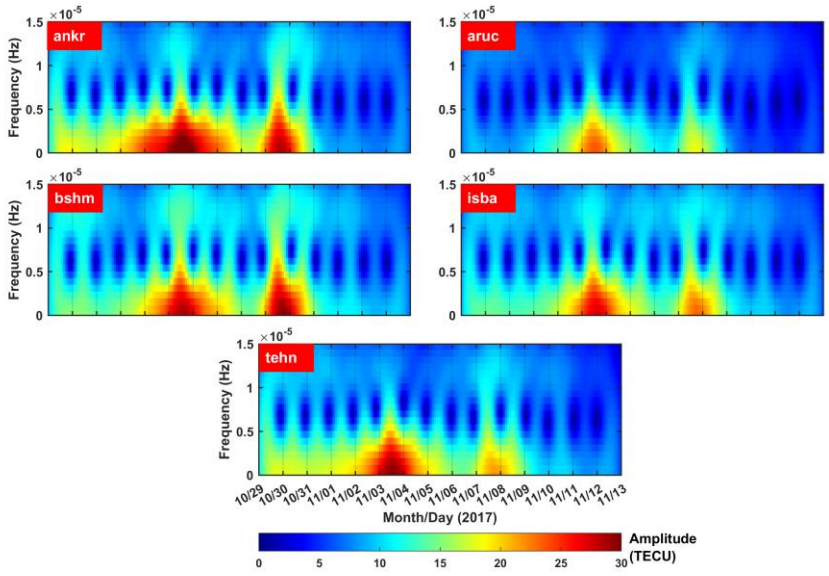

3. From Figure 5, I didn't find anomalies up to 4 TECu, nor from Figure 4 (as stated in the Conclusion). Please, clarify what is a maximum absolute deviation/anomaly value found and if it is higher than expected threshold for the calculation of vTEC.

- We revised as 1-3 TECu in all text.
- These values statistically represent the values outside the 95% confidence intervals of the normal distribution curve. Even if we assume that there are systematic errors in GPS TEC values, these errors remain within the distribution curve.

4. Authors may consider moving Figure 10 and appropriate discussion to Section 3, instead of discussing data analysis results in the Conclusion.

- We opened a new section as Section 3.4 with a headline **"The Prompt Penetration Electric Fields (PPEFs) Variation in Abnormal Days"**. We added Figure 10 and related explanations to this section.

5. Please, consider introducing all abbreviations in the text (not only in the abstract), e.g., LMTF, CMONOC, IGS, GIM etc., along with indexes in paragraph 80 (IMF, Ey, Vsw).

- All abbreviations in the text were introduced.

6. Please revise paragraphs 25-60, as they discuss studies that are related to both post-seismic (acoustic-gravity driven disturbances in the ionosphere) and pre-seismic activity. These are 2 completely different fields of studies and this should be clarified for readers not familiar with the topic (instead, the discussion of post-seismic studies may be fully excluded from the text).

- We removed the paragraph from L24 to L29 which is including a lot of citation related to post-seismic (acoustic-gravity driven disturbances in the ionosphere) activity.

7. Paragraph 205-210 – Should it be November instead of October?

- The typo was corrected as "November".

8. Figure 1 – Should it be the indication of the northern hemisphere latitudes as N (not K)?

- The typo was corrected. The new version of Fig. 1 is below.

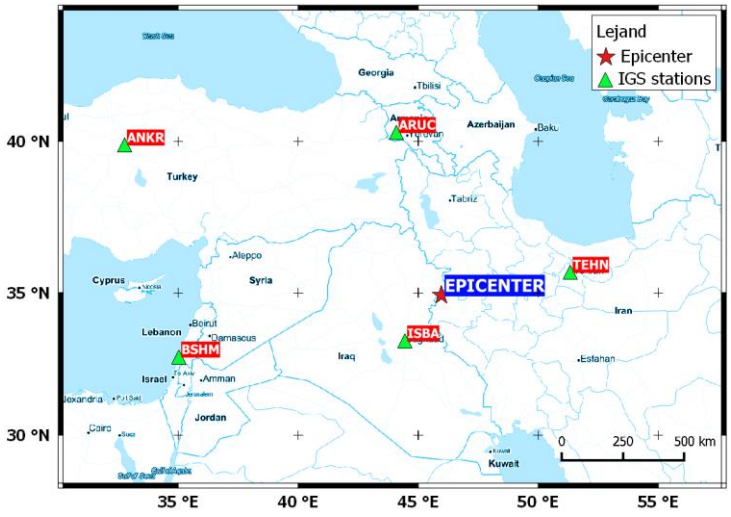

9. Why abnormal TEC variations are seen 8-9 days after the earthquake and not in closer dates? What is a physical explanation authors may suggest for this?

- We added possible physical explanations about the earthquake-ionosphere coupling to the introduction section of the article. There is not enough data in the study to make another comment on the physical explanation. Also, some researchers indicated the pre-earthquake ionospheric anomalies about 1-10 days before earthquakes (Xia et al., 2011; Inyurt et al., 2019, etc.).

RESPONSE TO REVIEWER#2

The manuscript presents an observational study of the ionospheric TEC precursors of the 12 November 2017 Iran-Iraq Border Earthquake. The study analyzed the TEC data from IGS stations surrounding the epicenter and the CODE GIMs using Short-time Fourier Transform method and a running median process. The study also analyzed space weather data to determine the contribution of geomagnetic activities to the TEC anomalies before the earthquake. The outcome of the study showed two groups of TEC anomalies with different causes: the anomalies 1-6 days before the earthquake were caused by a geomagnetic storm, while the anomalies 8-9 before the earthquake were related to the earthquake.

I find the manuscript fairly well-written in general. The study delivers interesting science results and would be inspiring to the community. In particular, the study presents a very nice demonstration of separating the space weather contribution from the earthquake contribution to TEC anomalies. However, there are certain ambiguities in methodology and results that need to be addressed, which are listed below.

- Thank you for your favorable comments, your time and consideration.

1. The relation between the TEC anomalies on November 3-4 and the earthquake is weak given the evidence shown in the manuscript. The authors claim that the TEC anomalies on November 3-4 are earthquake precursors because of quiet space weather, local dispersion and proximity to the epicenter. Instead of quiet space weather, Figure 3 shows a mild geomagnetic activity on November 3-4, with elevated Kp comparing to days immediately before and after. Is it possible that the TEC anomalies on November 3-4 are due to this mild geomagnetic activity? To exclude this possibility, the authors have shown a) the localized anomaly on GIMs of November 3-4, and b) the negligible variations of prompt penetration electric fields on November 3-4.

For a), GIMs are interpolated GNSS TEC maps. It is not clear how many and where the GNSS stations are in generating the GIMs. Are the five IGS stations surrounding the epicenter included for the GIMs? To directly demonstrate that the TEC anomalies on November 3-4 are localized, why not show the lack of anomalies for IGS stations further away from the epicenter (outside of the earthquake preparation area), using the exact same methodology for analyzing the existing 5 stations? A few more panels on Figure 5 for other stations would say it all.

- We analyzed the TEC data of two stations outside the earthquake preparation area and presented the results in Figure 5. In addition, we revised Figure 1 and some sections in the article in accordance with the new situation. The revised version of Figure 1 and Figure 5 are in below.
- In addition, we explained the relationship between GNSS TEC and GIM TEC in the first part of the reply to Reviewer#1. Please check it.

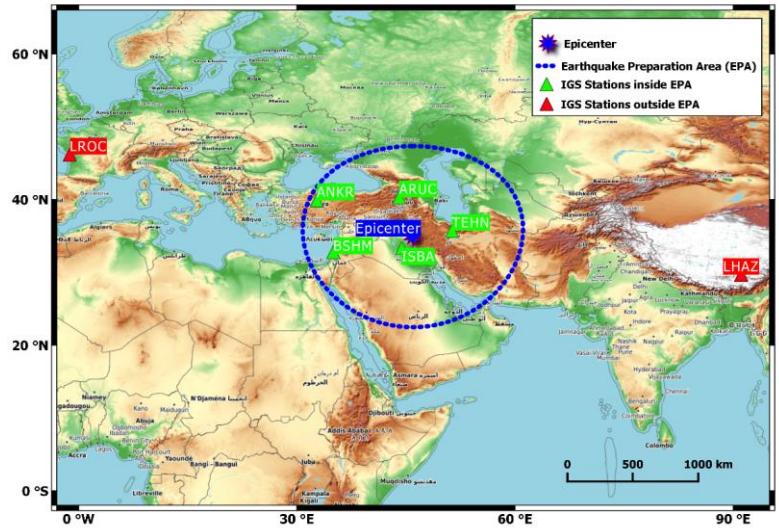

Figure: Revised version of Figure 1.

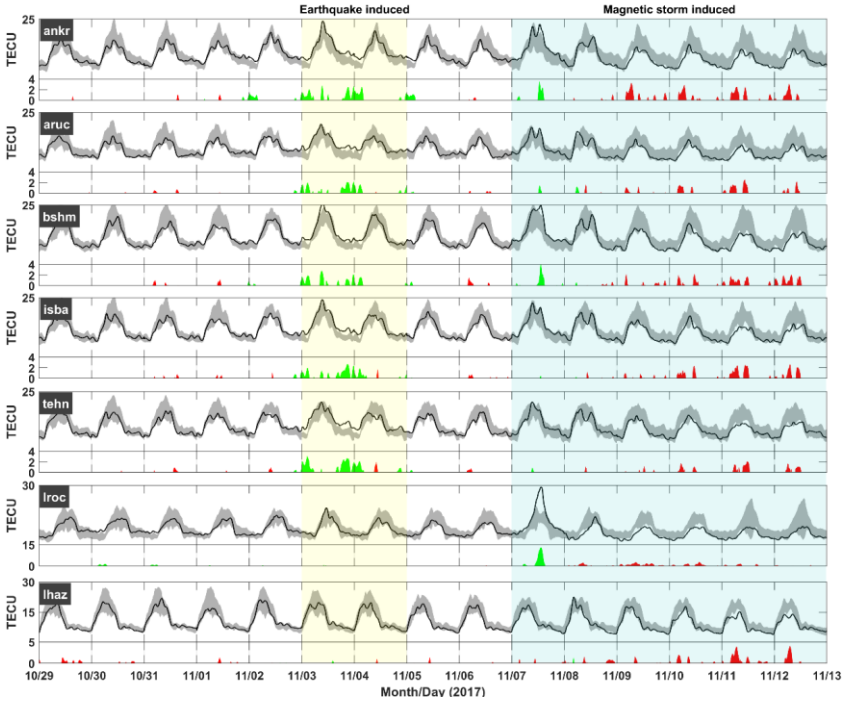

Figure: Revised version of Figure 5.

For b), I could not find how the PPEFs are calculated and what is the "Quiet" curve in Figure 10. Does the variation of PPEFs correlate with the TEC variations due to space weather? More explanation would be helpful.

- We included the explanations about PPEFs as a separate section (Section 3.4 with a headline "The Prompt Penetration Electric Fields (PPEFs) Variation in Abnormal Days") with the recommendation of Reviewer#1, and made the first paragraph of this section according to your recommendation as follows.
- *"The PPEFs is the prompt reaction of the equatorial zonal electric field to solar wind alteration, which is component of the interplanetary electric field (IEF) and the equatorial zonal electric field (Manoj et al., 2008). The penetration part of PPEFs (green line in Fig. 10) is calculated by the interplanetary data which is provided by the OMNI web site. Also, the quiet (climatological) part of PPEFs (violet line in Fig. 10) is equal to the 81-day moving average of F10.7 cm solar flux (Manoj and Maus, 2012)."*

2. Have the authors look into the wave characteristics, for instance the wave period/frequency and duration of the TEC anomalies on November 3-4? Are they similar to the characteristics of earthquake TEC precursors found in previous studies? This would better support the argument that the TEC anomalies on November 3-4 are the earthquake precursors.

- I applied the STFT method to the TEC time series for the first time in the article related to Van EQ and achieved successful results similar to the results of Iran-Iraq EQ. We compared the success of the STFT with the classical method (running median). The results are consistent. The STFT only shows anomalies in the TEC time series. As known, more analysis is needed as was done in the study to establish the relationship between the anomalies and the earthquake.

"Şentürk, E., Livaoğlu, H., Çepni, M. S. (2019). A Comprehensive Analysis of Ionospheric Anomalies before the M w 7· 1 Van Earthquake on 23 October 2011. The Journal of Navigation, 72(3), 702-720."

3. Line 15: molecules are separated into positively charged particles and electrons?

- To make it more understandable, we revised this section as follows: *"When molecules are exposed to light energy emitted from the sun, their components are divided into atoms, which are electrons and a compact nucleus of protons and neutrons. Negatively charged electrons effect the propagation of electromagnetic signals traveling between space and earth."*

4. Second paragraph of Introduction: some of the references are for ionospheric anomalies during and after earthquakes, which has very different physical mechanisms from the earthquake precursors. I noticed that referee #1 has also pointed this out. I hope the authors successfully address this in the paper revision.

- We removed the paragraph from L24 to L29 which is including a lot of citation related to co-seismic and post-seismic (acoustic-gravity driven disturbances in the ionosphere) activity.

5. Line 46 and Line 79: GIM and STFT are not defined in the main text.

- We defined them in the new version of the manuscript.

6. Line 95: Any references for CODE GIM?

- A citation added for CODE GIM at L100.